Astron. Astrophys. 325, 542–550 (1997)

ASTRONOMY
AND
ASTROPHYSICS

# Cold dust around Herbig–Haro energy sources: morphology and new protostellar candidates

**R. Chini**[1], **Bo Reipurth**[2], **A. Sievers**[3], **D.Ward-Thompson**[4], **C.G.T. Haslam**[5], **E. Kreysa**[5], **and R. Lemke**[6]
[1] Astronomisches Institut der Ruhr-Universität Bochum, Universitätsstr.150/NA 7, D-44780 Bochum, Germany
[2] European Southern Observatory, Casilla 19001, Santiago 19, Chile
[3] IRAM, Avda Divina Pastora 7, Nucleo Central, E-18012 Granada, Spain
[4] Royal Observatory, Blackford Hill, Edinburgh EH9 3HJ, UK
[5] Max-Planck-Institut für Radioastronomie, Auf dem Hügel 69, D-53121 Bonn, Germany
[6] Onsala Space Observatory, S-43992 Onsala, Sweden

Received 23 December 1996 / Accepted 20 April 1997

**Abstract.** We present 1300 $\mu$m maps of regions centered on the energy sources of 20 HH objects in order to study the distribution of circumstellar matter around these young stellar objects. The data show that the emission generally originates from a rather compact region which is embedded in a more diffuse environment. The relative contribution of the compact component to the total emission varies from 15 to 100%. About half of the compact components appear spherically symmetric while the other half displays an elongated structure. There is, however, no correlation between the optical jet axis and the flattened dust structures, indicating that collimation occurs on smaller scales. Close to the energy source of HH 114 we discovered a so far unknown mm–source with $L_{bol}/L_{smm} < 100$ suggesting that it is still in its early protostellar evolutionary stage. In three other regions we detected similar unknown mm–sources without *IRAS* counterparts, indicating that they are also likely new protostellar candidates.

**Key words:** interstellar medium: dust – stars: circumstellar matter – formation of

## 1. Introduction

Herbig-Haro (HH) objects are shocks which trace bipolar supersonic outflows from young stars in the process of building up their masses through accretion. They are ubiquitous in star forming molecular clouds, and their presence signals a recent nearby star birth.

Most HH driving energy sources are deeply embedded in placental material. In an earlier paper, Reipurth et al. (1993a, hereafter Paper I) obtained 1300 $\mu$m photometry of 59 HH energy sources, and demonstrated that they are surrounded by considerable amounts of cold (36K) circumstellar material, typically in the range from a few tenths to several solar masses. It was concluded that HH energy sources, as a class, are among the youngest stellar objects known.

With the advent of sensitive array detectors on large radio telescopes it has become feasible to map the structure and environment of large numbers of newborn stars in the mm radio continuum. Interferometer maps are less ideal for this, partly because of practical time constraints, but also because extended emission tends to be filtered out. In this paper we discuss the structure of the massive dust envelopes of HH energy sources based on detailed 1300 $\mu$m maps of 20 of the sources we detected in Paper I.

The large areas covered by our maps have permitted us to additionally search for hitherto unknown protostellar sources in the neighborhood of the central HH energy sources. Because star formation tends to occur in groups, we believe that the most effective way of finding such protostars is to survey the cloud regions immediately around very young stars, and this search strategy has been borne out by the discovery of several protostellar candidates in our recent surveys (Chini et al. 1993, Reipurth et al. 1996).

## 2. Observations

The 1300 $\mu$m mapping was carried out at the IRAM 30 m telescope during two bolometer sessions in February 1993 and March/April 1995. In the first session we used the MPIfR 7–channel bolometer array. The atmospheric conditions were good to average with an optical depth between 0.15 and 0.26; the pointing was stable, giving an accuracy of about 3″ rms. The calibration was mainly done on Mars (3 maps) and Uranus (1 map). The overall system sensitivity was 50 mJy Hz$^{-1/2}$. Typi-

*Send offprint requests to*: R. Chini

**Table 1.** 1300 $\mu$m mapping of HH energy sources

| HH | Source | $RA$ | $Dec$ | $a$ | $b$ | $a/b$ | $S_{\rm source}$ | | $S_{\rm total}$ | |
|---|---|---|---|---|---|---|---|---|---|---|
| | | [1950] | | | | | [mJy] | | [mJy] | |
| (1) | (2) | (3) | (4) | (5) | (6) | (7) | (8) | (9) | (10) | (11) |
| | HH 7-11 MMS3 | 03 25 56.67 | +31 05 17.4 | 13.3 | 4.2 | 3.2 | 300 | 487 | .... | ... |
| | HH 7-11 MMS2 | 03 25 57.55 | +31 05 30.1 | 6.9 | 5.3 | 1.3 | 904 | 1184 | 3861 | 543 |
| HH 7-11 | HH 7-11 MMS1 | 03 25 58.19 | +31 05 41.1 | 10.7 | 5.8 | 1.8 | 1108 | 1743 | ..... | ... |
| HH 6 | HH 6 VLA | 03 26 05.78 | +31 08 11.2 | 16.8 | 7.4 | 2.3 | 414 | 839 | 2380 | 360 |
| HH 28-29 | L 1551 IRS 5 | 04 28 40.27 | +18 01 41.6 | 10.0 | 7.0 | 1.4 | 1640 | 2469 | 4990 | 627 |
| HH 150 | HL Tau | 04 28 44.44 | +18 07 34.9 | 4.7 | 3.4 | 1.4 | 1110 | 1233 | 1258 | 158 |
| | HH 114 MMS | 05 15 33.45 | +07 08 52.9 | 7.8 | 5.4 | 1.4 | 712 | 940 | 1216 | 157 |
| HH 114 | HH 114 IRAS | 05 15 35.72 | +07 07 51.9 | 17.0 | 9.8 | 1.7 | 342 | 765 | 2242 | 319 |
| HH 240 | RNO 40 IRS | 05 17 21.40 | −05 55 06.1 | 11.9 | 6.0 | 2.0 | 116 | 195 | 1230 | 166 |
| HH 243 | RNO 43 IRS | 05 29 30.74 | +12 47 34.3 | 9.3 | $<1$ | $>9$ | 279 | 359 | 611 | 94 |
| HH 34 | HH 34 IRS | 05 33 03.64 | −06 28 52.0 | 7.8 | $<1$ | $>8$ | 367 | 434 | 1309 | 207 |
| | HH 1-2 MMS3 | 05 33 52.35 | −06 47 34.4 | 21.8 | 17.7 | 1.2 | 193 | 810 | .... | ... |
| | HH 1-2 MMS2 | 05 33 52.96 | −06 47 14.8 | 15.5 | 10.8 | 1.4 | 247 | 597 | 2082 | 228 |
| HH 1-2 | HH 1-2 MMS1 | 05 33 57.15 | −06 47 57.8 | 8.7 | 7.6 | 1.1 | 325 | 504 | 3300 | 362 |
| HH 147 | HH 147 MMS | 05 33 59.24 | −06 46 31.1 | 22.2 | 10.4 | 2.1 | 120 | 374 | 1967 | 227 |
| HH 65 | Re 50 IRS | 05 38 02.49 | −07 28 58.3 | 10.8 | 9.4 | 1.1 | 206 | 308 | 1296 | 163 |
| HH 212 | IRAS 05413-0104 | 05 41 18.84 | −01 04 10.8 | 11.9 | 8.7 | 1.4 | 154 | 289 | 657 | 100 |
| HH 111 | HH 111 VLA | 05 49 09.41 | +02 47 48.6 | 9.8 | 7.8 | 1.3 | 545 | 839 | 1392 | 209 |
| HH 160 | ZCMa | 07 01 22.75 | −11 28 36.8 | 18.3 | 13.0 | 1.4 | 357 | 961 | 1277 | 194 |
| HH 224 | SR 24 | 16 23 56.64 | −24 38 54.3 | 6.9 | 4.8 | 1.4 | 217 | 280 | 254 | 36 |
| HH 80-81 | IRAS 18162-2048 | 18 16 13.30 | −20 48 47.0 | 15.0 | 12.7 | 1.2 | 1469 | 3428 | 7107 | 904 |
| HH 106-107 | ESO $H_\alpha$ 279 | 18 26 59.69 | +01 16 42.7 | 14.1 | $<4$ | $>4$ | 69 | 119 | 816 | 115 |
| | HH 108 IRAS | 18 33 07.76 | −00 35 48.4 | 10.2 | 5.9 | 1.7 | 265 | 411 | 528 | 68 |
| HH 108 | HH 108 MMS | 18 33 12.11 | −00 35 21.7 | 10.1 | 7.1 | 1.4 | 175 | 282 | 228 | 32 |
| HH 223 | IRAS 19156+1906 | 19 15 42.06 | +19 06 51.0 | 14.8 | 11.3 | 1.3 | 310 | 678 | 668 | 95 |
| HH 119 | B 335 IRS | 19 34 35.14 | +07 27 21.0 | 15.5 | 11.5 | 1.3 | 314 | 709 | 1009 | 148 |
| HH 165 | 1548C27 | 19 40 47.18 | +23 17 02.9 | 27.1 | 22.2 | 1.2 | 169 | 1015 | 1677 | 218 |

Notes to Table 1: (1) HH number (2) Most common name of the driving source. (3,4) Source position from Gaussian fit. (5,6,7) Major and minor axis of the compact component and their ratio. (8) Peak flux in 11″. (9) Source flux from Gaussian fit. (10) Total flux within the lowest significant contour; for HH 7-11 this flux comprises all 3 sources, for HH 1-2 it refers to MMS2 and MMS3. (11) Error of total flux.

cal map sizes were 2′ by 2′ (in Az,El), some were larger with 3′ by 3′. We used wobbler throws of 32″ or 44″; the beam size of a single channel was 11″ (HPBW). The mapping was carried out at a scanning speed of 4″/s with a separation of 4″ between the scanning lines.

During the second session we had the opportunity to use the MPIfR 19–channel bolometer. The atmosperic conditions were similar, with $\tau$–values between 0.16 and 0.3. The pointing accuracy was about 3″ rms. Mars (2 maps) and Uranus (2 maps) served again as calibration standards. The sensitivity was slightly better than in the previous run, giving about 40 mJy Hz$^{-1/2}$. The map sizes were 3′ by 3′, the wobbler throw was set to 32″ and the beam size was again 11″ (HPBW). We worked at a scanning speed of 5″/s and the scanning lines were separated by 4″. We estimate our absolute photometric accuracy at 1300 $\mu$m to be of the order 20%.

The 350 to 2000 $\mu$m photometry for HH 114 MMS was performed at the James Clerk Maxwell Telescope[1](JCMT) on Mauna Kea, Hawaii, from February 25 until March 1, 1994. The detector was the UKT14 receiver (Duncan et al. 1990). Observations were carried out with a constant aperture of about 18″. The secondary mirror was chopped in azimuth at $\sim$ 7 Hz with a beam separation of 70″. Calibration was performed by measuring Uranus (Orton et al. 1986, Griffin & Orton 1993), and the secondary calibrators NGC 2071IR and W3(OH)(Sandell 1994). We used a similar calibration method to that outlined by Stevens & Robson (1994). The 225 GHz opacity at zenith was $0.027 \leq \tau \leq 0.040$ and remained stable throughout a single shift. We estimate our total absolute calibration uncertainty for the JCMT observations to be $\sim$ 30%. Pointing and focus checks were performed typically once per hour.

The *IRAS* Point Source Catalog lists flux densities for HH 114 (*IRAS* 05155+0707) at all four wavebands. However, this source is not coincident with HH 114 MMS. Therefore we obtained the *IRAS* Calibrated Reconstructed Detector Data

[1] The James Clerk Maxwell Telescope is operated by the Royal Observatory, Edinburgh, on behalf of the United Kingdom Particle Physics and Astronomy Research Council (PPARC), the Netherlands Organisation for the Advancement of Pure Research (NWO) and the Canadian National Research Council (NRC).

**Table 2.** FIR and submm photometry of HH 114 MMS.

| $\lambda$ [$\mu$m] | S [Jy] |
|---|---|
| 12 | $<$ 2 |
| 25 | $<$ 5 |
| 60 | $<$ 30 |
| 100 | $<$ 90 |
| 350 | 16.7 |
| 450 | 7.7 |
| 800 | 2.1 |
| 1100 | 0.88 |
| 1300 | 0.61 |
| 2000 | 0.26 |

Notes to Table 2: The 12 to 100 $\mu$m 3 $\sigma$ upper limits were measured from the *IRAS* raw data, the 350 to 2000 $\mu$m measurements were made with the JCMT and refer to an 18″ aperture. Absolute calibration errors are estimated to be 30%.

(CRDD) of the region, which consists of the time sequence data streams from each detector (for details of the *IRAS* focal plane detector arrangement see Fig. II.C.6 of Beichman et al. 1988), and made images from the individual *IRAS* detectors using the UK Starlink software package IRAS90 (e.g. Ward-Thompson et al. 1989; Ward-Thompson & Robson 1990). We failed to find a point source coincident with HH 114 MMS, but we performed photometry on these data using a 3′ aperture, and thereby estimated upper limits to the *IRAS* flux densities of HH 114 MMS.

We selected the strongest sources from Paper I and included HH 212 in the present investigation. Table 1 gives the positions and various 1300 $\mu$m flux densities of all sources as derived from Gaussian fits to the maps in Fig. 6. Table 2 contains the FIR and submm fluxes for HH 114 MMS. When comparing $S_{\rm source}$ (column 9) in Table 1 with the corresponding flux densities of Paper I, one finds on the average that the new values tend to be higher than the old ones. This is partly due to a combination of a better positional accuracy and a better background subtraction, both obtained by the mapping procedure. In addtion, some extended sources could not be measured properly by the earlier single beam ON-OFF measurements. While this increase in flux has no influence on the luminosity of the sources as quoted in Paper I, the dust mass has to be increased formally by about 50% for some of the sources. Taking into account, however, that the unknown dust properties in these dense environments introduce an error that might be a factor 5 to 10 above the standard values, we do not consider it necessary to recalculate the corresponding dust masses. The conclusion of Paper I, concerning the flat shape of the spectral energy distributions is even strengthened by the increase of the 1300 $\mu$m flux densities.

## 3. Individual regions

In this section we discuss four individual regions in detail because there we have detected new mm–continuum sources. Descriptions of the other regions in Table 1 can be found in Reipurth (1994).

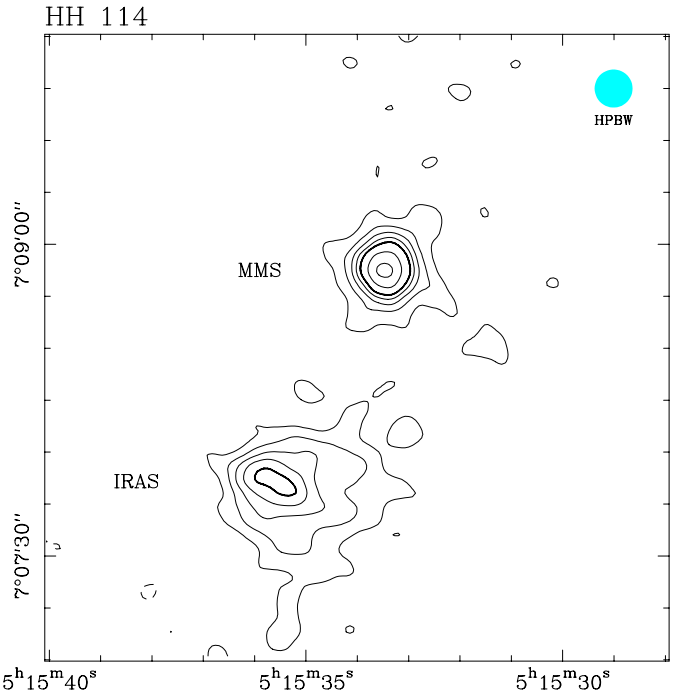


**Fig. 1.** 1300 $\mu$m continuum map of the region around HH 114, displaying the *IRAS* source and new mm source. Contour levels are -80, 80 to 400 by 80, 560, 720 mJy. Coordinates are epoch 1950.

### *3.1. HH 114*

The molecular shell surrounding the young massive star $\lambda$ Orionis is a region rich in newborn stars and associated Herbig-Haro objects. Among the outflows is a giant HH complex, HH 114-115, comprising two bow shocks with a separation of 2.4 pc. The two HH objects are located on either side of a Class I FIR source *IRAS* 051555+0707 (Reipurth et al. 1997).

We have mapped the source region at 1300 $\mu$m, and detected *IRAS* 05155+0707, see Fig. 1. In addition, we have discovered another, hitherto unknown source 1.5′ to the north–west, which we here call HH 114 MMS. As discussed in Sect. 2, this new source is not detected by *IRAS*, and suspecting that we here have a protostellar candidate, we obtained the submm photometry from the JCMT listed in Table 2. In the following we discuss the nature of HH 114 MMS based on these data.

The spectral energy distribution of HH 114 MMS is shown in Fig. 2. As a first guess one may assume that the emission arises from dust at a single temperature. In this case we can fit the spectrum by a greybody of the form

$$S_\nu = \Omega\, B_\nu(T_{\rm d})\,(1 - e^{-\tau}), \qquad (1)$$

where $\Omega$ is the solid angle of the emitting region, $B_\nu$ is the Planck function and $\tau$ is the optical depth approximated by $\tau = (\nu/\nu_{\rm c})^\beta$; $\nu_{\rm c}$ denotes the critical frequency where the optical depth is 1. The best fit to the data is shown by the solid curve in Fig. 2 and corresponds to $\beta$ = 1.0 and $T_{\rm d}$ = 28 K. The $\beta$–value is rather well determined by the data at longer wavelengths whereas the short submm wavelengths together with the *IRAS* 60 $\mu$m limit constrain the temperature to a certain degree. This

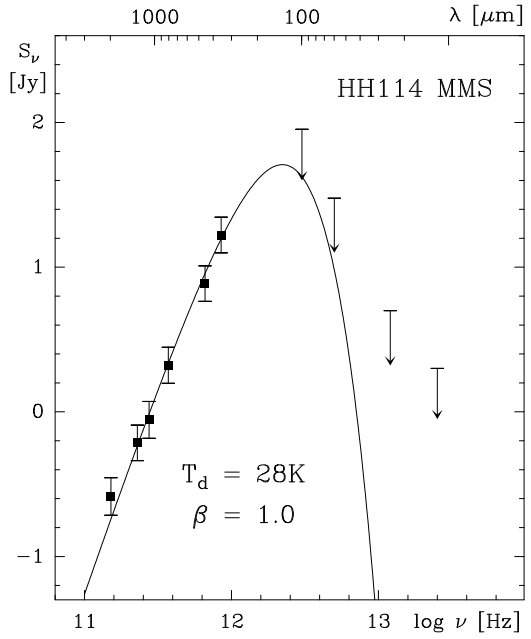


**Fig. 2.** Spectral energy distribution of HH 114 MMS. The solid curve is a greybody fit with a dust temperature $T_{\rm d}$ = 28 K and $\beta$ = 1.0.

extraordinary flat spectrum may originate from dust at a range of temperatures where part of the emission is optically thick and/or from dust grains with unusual optical properties. In any case the spectral properties of this source are very similar to the protostellar condensation HH 24 MMS (Chini et al. 1993, Ward-Thompson et al. 1995).

In order to determine the evolutionary stage of HH 114 MMS we calculate the bolometric luminosity $L_{bol}$ as the energy output from 12 to 2000 $\mu$m; the submm luminosity $L_{smm}$ is the energy emitted at $\lambda \geq 350\,\mu$m. As suggested by André et al. (1993), a ratio $L_{bol}/L_{smm} < 200$ is characteristic for Class 0 sources. In the case of HH 114 MMS we can only derive upper limits for $L_{bol}$ and $L_{bol}/L_{smm}$ because of the upper limits from *IRAS*. But even taking the numbers in Table 2 at their face value we obtain $L_{bol}$ = 26.3 $L_\odot$ and $L_{smm}$ = 0.3 $L_\odot$ and thus $L_{bol}/L_{smm} \sim 90$, indicating that the source must be still in an early protostellar phase.

Under the assumption of optically thin emission we may estimate the total amount of mass associated with HH 114 MMS from the flux density at 1300 $\mu$m according to

$$M_{\rm gas} = S_\nu\, \kappa_\nu^{-1}\, B_\nu(T_{\rm d})^{-1}\, D^2 \qquad (2)$$

As outlined by Ward-Thompson et al. (1995) the dust properties in protostellar sources are likely to be different than those in the diffuse interstellar medium, resulting in larger-than-normal fluffy grains. We therefore use an enhanced mass absorption cross section $\kappa_{1300} \simeq 0.02\,{\rm cm}^2$ per gram of interstellar matter. The total mass is then 5.5 $M_\odot$ at an assumed distance of 460 pc.

Following our discovery of HH 114 MMS, we mapped the region at 3.6 cm at the VLA, and in addition to detecting *IRAS* 05155+0707, we found a source with a flux of 0.13 mJy only 4.4″ from our mm position of HH 114 MMS, which is within the positional errors (Rodriguez & Reipurth 1996). The VLA position is $\alpha_{1950}$ 05:15:33.22 $\delta_{1950}$ = 07:08:55.6. So HH 114 MMS can be added to the growing list of Class 0 sources, which are detectable at centimeter wavelengths. The 3.6 cm flux lies a factor of 4 above the extrapolation of the fit in Fig. 2. At present it is impossible to distinguish whether this means a flattening of the dust emission spectrum at mm and cm wavelengths or simply involves a new emission component originating from a shock front.

The question arises which of the two sources, HH 114 *IRAS* or HH 114 MMS, is the driving source of the giant HH 114-115 complex. Unfortunately, the two sources lie more or less on a northwest-southeast line, which is also the direction of the HH flow, so on geometric grounds we cannot favor one over the other.

### *3.2. The HH 1-2 region*

Since their discovery by Herbig (1951) and Haro (1952), the Herbig-Haro objects HH 1 and HH 2 have been extensively studied and have emerged as the prototypical bipolar HH flow (see, e.g. Solf et al. 1989 and references therein). They are driven by a deeply embedded source, VLA 1, detected by Pravdo et al. (1985) and with a far–infrared luminosity of about 50 $L_\odot$ (Harvey et al. 1986). Recently, a new collimated HH flow, HH 144, was discovered emerging at a large angle to the HH 1-2 flow from a source, VLA 2, displaced by only 3″ from VLA 1, suggesting that they form a young binary (Reipurth et al. 1993b).

The region around the VLA 1/2 sources is rich in young objects. The central star is an optically visible T Tauri star (Cohen & Schwartz 1979), an $H_2O$ maser was found south-west of HH 1 (Lo et al. 1975, Haschick et al. 1983), an infrared source is associated with HH 3 (Roth et al. 1989), and a number of *IRAS* sources were found by Pravdo & Chester (1987).

Our 1300 $\mu$m continuum map is shown in Fig. 3. It reveals the presence of a number of sources; their positions and fluxes are listed in Table 1. Reipurth et al. (1993a) detected a strong mm/submm source ($S_{870}$ = 1672 mJy, $S_{1300}$ = 645 mJy) at the position of the VLA source. It is seen in Fig. 3 as a slightly elongated source, MMS1, and is the brightest one in the map. In addition to this, the map shows a ridge, 17″ SSW of MMS1. At our spatial resolution of 11″, MMS1 and the ridge are not fully separated but being present in each of our individual maps, the reality of the ridge is beyond doubt. MMS1 and the ridge are embedded in a faint extended halo.

The position of MMS1 is 6″ SSE of the VLA 1 radio position. The internal accuracy between our individual maps is 1.5″. Likewise, maps of the region from previous observing runs show a similar offset so that we have no evidence to attribute this difference to a pointing error. Nevertheless, taking into account our pointing accuracy we cannot exclude that MMS1 and VLA 1 (plus VLA 2) are the same object.

MMS1 and its SSW ridge are located in a dense cloud core detected in $NH_3$ by Torrelles et al. (1985), in CS by Cernicharo (1991) and in $H_2CO$ by Davis et al. (1990). More detailed observations of the $NH_3$ (1,1) and (2,2) transitions show an intri-

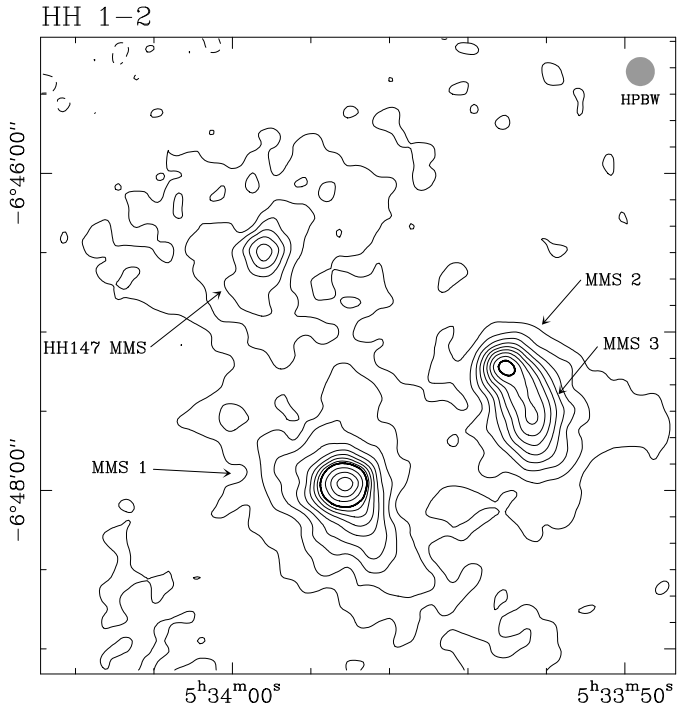


**Fig. 3.** 1300 $\mu$m continuum map of the region around HH 1-2. Contour levels are -30, 30 to 270 by 30, 270 to 450 by 60 mJy. Coordinates are epoch 1950.

cate morphology with an overall elongated shape perpendicular to the HH 1-2 flow axis and a complex kinematics (Martin-Pintado & Cernicharo 1987, Marcaide et al. 1988, Rodriguez et al. 1990a).

MMS1 is situated centrally in the dense elongated molecular core in what appears to be an evacuated region. The SSW ridge, on the other hand, is found towards one of the densest parts of the south-western ammonia lobe. The halo seen in the continuum at 1300 $\mu$m coincides rather well with this south-western lobe. It thus appears that the ridge could represent a secondary star formation event in the dense material left over from the formation of the VLA 1 and 2 system. Whereas both of these VLA sources actively drive HH flows, there is no evidence for HH objects driven by sources in the ridge (Reipurth et al. 1993b).

A two–dimensional Gaussian fit to MMS1, after subtraction of the ridge, shows that it is marginally resolved, with major and minor axes of 17.4″ and 15.1″, respectively, and a position angle of the major axis of 298°. At 460 pc distance, this corresponds to a major axis of 8000 AU. If real, this suggests that MMS1 still has an extended dust envelope surrounding it, presumably a vestige of the collapsing cloud fragment which formed the young stars VLA 1 and 2. The spectral energy distribution measured by Reipurth et al. (1993a) suggests a dust temperature of $\sim$ 36 K and a $\beta$ of $\sim$ 1.0; the dust envelope is thus warmer than expected for a true protostar. We also note that the position angle of the minor axis is close to the position angle of 148 degrees for the HH 1-2 flow, which leads us to speculate that the dust envelope is either flattened, or the "top and bottom" have been blown off by the collimated outflow.

In addition to MMS1, Fig. 3 shows another source (MMS2) about 80″ to the northwest. In this region, Lo et al. (1975) and Haschick et al. (1983) found an $H_2O$ maser. VLA observations have revealed two 6 cm radio continuum sources here, one is coincident with the $H_2O$ maser (Pravdo et al. 1985), and the other, only 5″ further southwest, shows pronounced time variability (Rodriguez et al. 1990b). A near–, mid– and far–infrared source detected by Harvey et al. (1986), with a total luminosity of 70 $L_\odot$, is coincident with the $H_2O$ maser source, and was imaged in the near–infrared by Roth et al. (1989). Our continuum source, MMS2, is displaced by about 5″ to the SE from the two VLA sources, similar to MMS1 and VLA 1. The $NH_3$ map of Rodriguez et al. (1990a) and the CS observations of Cernicharo (1991) show that MMS2 is located close to a region of high density. Indeed, the more detailed $NH_3$ map in the (2,2) transition of Torrelles et al. (1993) shows both sources at the center of a small dense cloud core.

A slightly fainter source, MMS3, is situated 20″ SSW of MMS2, in the center of the extended $NH_3$ cloud observed by Rodriguez et al. (1990a). There is no previous evidence for star formation in this region.

In the upper NE corner of Fig. 3 we find another 1300 $\mu$m source. In this region there is a faint HH object, HH 147, (Eislöffel et al. 1994), which moves away from a faint T Tauri star (No. 3 of Strom et al. 1985). This star coincides precisely with our 1300 $\mu$m source, here called HH 147 MMS.

### *3.3. HH 108-109*

The two HH objects HH 108 and 109 are located at the edge of a highly opaque sharp–edged cloud in Serpens (Reipurth & Eiroa 1992). They each have some morphological features which suggest that they may be bow shocks facing away from a source to the north–east. In that direction one finds the Class I *IRAS* source 18331–0035, with a projected separation of only 0.12 pc and 0.21 pc from HH 109 and HH 108, respectively, at the assumed distance of 310 pc. The axis of the two HH objects is very well aligned with a line through the *IRAS* source, which led Reipurth & Eiroa (1992) to conclude that the *IRAS* source was a good candidate for the driving source of the two HH objects.

Our 1300 $\mu$m map of the HH 108-109 source region is shown in Fig. 4. Two well defined sources are visible, the brighter with a total flux of 528 mJy and the fainter with 228 mJy. The angular distance between the two sources is 71″, corresponding to a projected separation of only 0.11 pc, or 22000 AU. The center of the uncertainty ellipse of *IRAS* 18331–0035 coincides within a few arcseconds with the position of the brighter mm-source, and they are without doubt identical. The fainter object, which we here call HH 108 MMS, is a new source in the region. We do not have submm photometry of this new source, but the fact that it is not seen by *IRAS*, and does not even cause a slight shift in the *IRAS* position of the nearby mm source, suggests that the new object is much fainter at *IRAS* wavelengths, possibly because it is colder than the *IRAS* source. We speculate that the

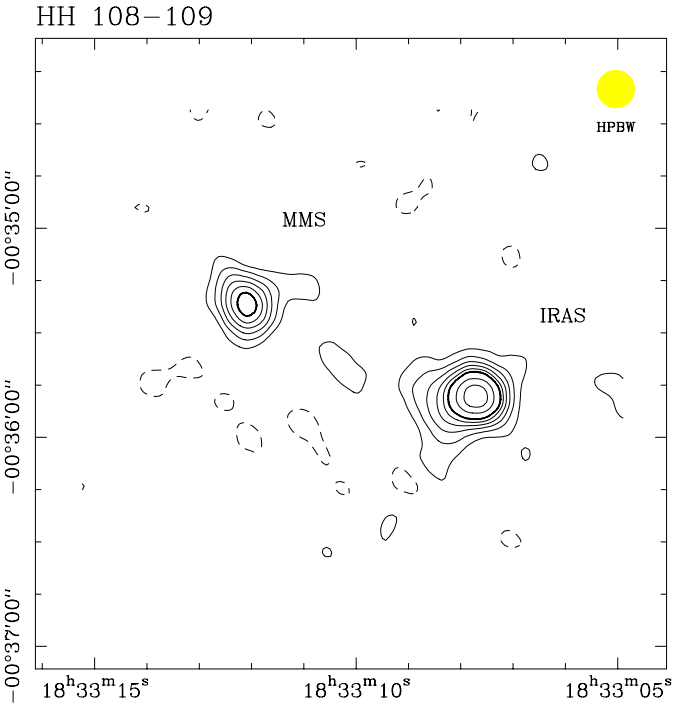


**Fig. 4.** 1300 $\mu$m continuum map of the region around HH 108-109 displaying the *IRAS* source and new mm source. Contour levels are -25, 25 to 150 by 25, 200, 250 mJy.

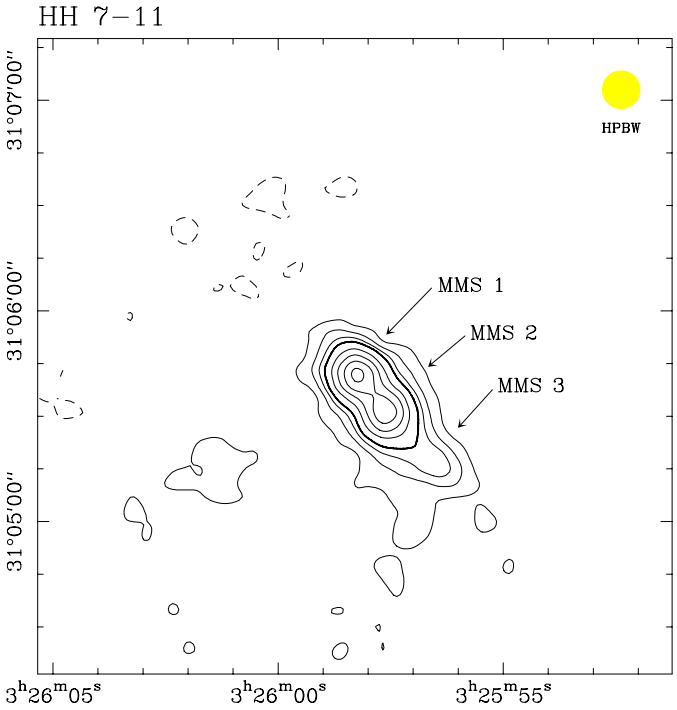


**Fig. 5.** 1300 $\mu$m continuum map of the region around HH 7-11. Contour levels are -100, 100 to 400 by 100, 400 to 1200 by 200 mJy. Coordinates are epoch 1950.

new source is similar to HH 24 MMS and HH 114 MMS and may be a protostellar object.

At present it is unclear which of these two sources is the more likely object to be driving the nearby HH objects because both lie close to the line defined by the two HH objects. Thus, further observations, for example in molecular hydrogen or in CO are required to identify the driving source.

### *3.4. HH 7-11*

The Herbig-Haro objects 7-11 are among the best studied such objects (e.g. Solf & Böhm 1987). They are located in the NGC 1333 region, which is rich in young stars and HH objects (e.g. Strom et al. 1976, Aspin et al. 1994, Bally et al. 1996), and at a distance of about 350 pc (Herbig & Jones 1983). The young visible star SVS 13 has long been assumed to be the driving source. A high velocity molecular outflow also streams from the source (e.g Koo 1989). Far–infrared mapping by Cohen et al. (1985) showed an elongated circumstellar structure.

The region has been mapped in the mm continuum by several groups. Grossman et al. (1987) did 2.7 and 3.1 mm aperture synthesis observations and detected two sources, one approximately coincident with SVS 13, and another about 15″ further southwest, also known as SVS 13B. Some controversy has arisen over the reality of this second source, since Woody et al. (1989) failed to detect it with interferometer observations at 1.4 mm, and similarly Sandell et al. (1990) did not detect it with single dish observations at 800 and 1100 $\mu$m.

In Fig. 5 we show our 1300 $\mu$m map of the region. We clearly see two well defined sources, separated by about 12″, or 4200 AU in projection at 350 pc. These sources coincide within a few arcseconds with the NE and SW sources of Grossman et al. (1987), which is within the positional uncertainties, and are certainly identical with these two sources, thus confirming their reality. As doubt is emerging that SVS 13 can really drive the powerful optical and molecular outflows in the region, we prefer to call these two sources for HH 7-11 MMS1 and 2, rather than SVS 13 and SVS 13B as done previously. It seems to us possible, and even likely, that SVS 13 is simply one of the multitude of young already visible and therefore more evolved young stars in the region, while MMS1 and 2 are deeply embedded, possibly protostellar,sources.

In addition to MMS1 and 2, we find yet another, albeit weaker source further to the southwest, MMS3, which approximately coincides with the location of a 6 cm radio continuum source ($03^h25^m56.38^s$, +31°05′20.3″) and an $H_2O$ maser ($03^h25^m56.6^s$, +31°05′19″) (source B of Haschick et al. 1980). It would be of great interest to observe these three embedded sources at submm wavelengths to ascertain their evolutionary stages.

In a recent study, Rodríguez et al. (1997) have performed sensitive, high angular resolution VLA observations at 3.6 cm and 6 cm. Their source VLA 4 precisely coincides with SVS 13. About 6″ SW of SVS 13 they detect a new VLA source, VLA 3, which aligns better with the HH flow axis than SVS 13. VLA 3 is itself elongated along the flow axis. Altogether VLA 3 is a more probable source of HH 7-11 than SVS 13. Rodríguez et

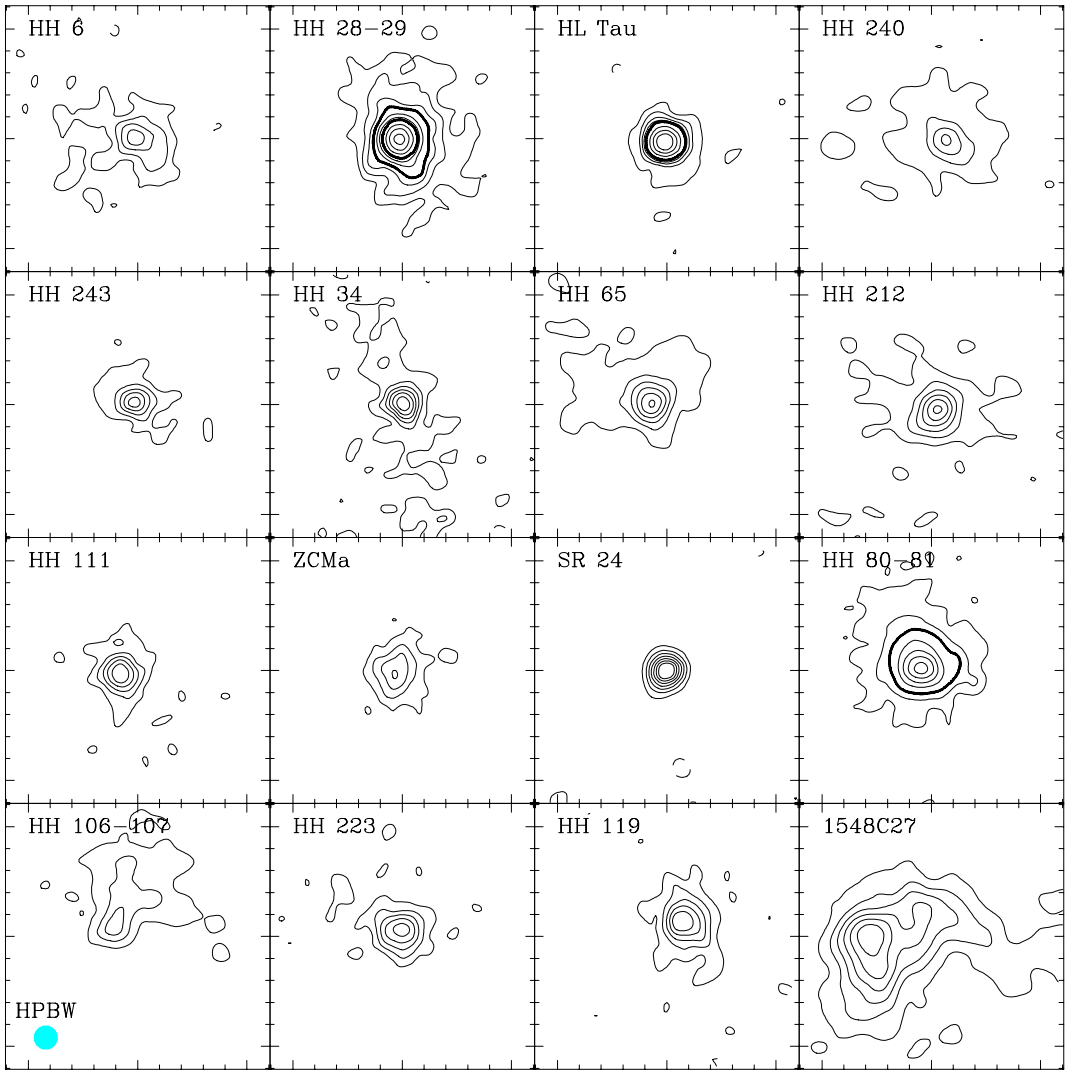


**Fig. 6.** 1300 $\mu$m continuum maps of 16 additional sources. Contour levels are: **HH 6** (-125, 125 to 500 by 125), **HH 28-29** (-80, 80 to 320 by 80, 480 to 800 by 160, 1100 to 1700 by 300), **HL Tau** (-60, 60 to 300 by 60, 300 to 900 by 200), **RNO 40** (-40, 40 to 160 by 40), **RNO 43** (-60, 60 to 300 by 60, **HH 34** (-60, 60 to 360 by 60), **HH 65** (-40, 40 to 240 by 40), **HH 212** (-30, 30 to 180 by 30), **HH 111** (100 to 500 by 100), **ZCMa** (-100, 100 to 400 by 100), **SR 24** (-25, 25 to 180 by 25), **HH 80-81** (-150, 150 to 450 by 150, 750 to 1650 by 300), **HH 106-107** (-25, 25 to 75 by 25), **L 723** (-60, 60 to 300 by 60), **HH 119** (-60, 60 to 300 by 60), **1548C27** (-30, 30 to 180 by 30) all in mJy; thick contours denote the change of spacing. The tick marks are separated by 12″.

al. (1997) also detect (their VLA 2) the above mentioned VLA source first noted by Haschick et al. (1980).

With our 1300 $\mu$m beam size of 11″ and a pointing accuracy of about 3″ it is not easy to compare the new VLA sources with our map. Although none of the mm and VLA sources precisely coincide, it is suggestive that they are related: An offset of 3″ WNW of our map leads to a perfect alignement of VLA 2 with MMS3 and VLA 3 with MMS1. MMS2 has no VLA counterpart. The coincidence of a strong mm continuum source with VLA 3 supports the suggestion by Rodríguez et al. (1997) that iy is VLA 3, rahter than SVS 13 (= VLA 4) which drives the HH 7-11 flow.

## 4. Morphology of dust emission

Fig. 6 shows the 1300 $\mu$m contours of the remaining sources. Most of them display a structure consisting of a rather compact but resolved source embedded in a more diffuse environment. We have included in Table 1 the 1300 $\mu$m flux density within an 11″ beam ($S_{\rm peak}$) centered on the peak of emission (column 8) as well as the total flux from the compact source ($S_{\rm source}$) as obtained from the Gaussian fit (column 9). The ratio $C = S_{\rm peak}/S_{\rm source}$ of both quantities reflects the central concentration of the emission, ranging from rather flat distributions with $C$ = 17% (1548C27) to highly peaked sources with $C$ = 90% (HL Tau). Neglecting the influence of a radial temperature gradient, $C$ measures the degree of condensation of the circumstellar

cloud into a more compact configuration, i.e. most probably into a disk.

The diffuse environment often attains a complicated structure, that does not resemble the shape of the compact component. The integrated 1300 $\mu$m flux within the lowest contour ($S_{\rm total}$) is given with its uncertainty in Table 1 (columns 10 and 11). Defining a new quantity $D = S_{\rm total}/S_{\rm source} - 1$, which ultimately measures the fraction of material left in the diffuse parental cloud, we find that $D$ ranges from 0% to 85%. In a few sources like HL Tau or SR 24 the entire emission is confined to the compact component whereas in sources like HH 106-107 up to 85% of the flux originates from the extended region. Comparing the degree of concentration $C$ of the inner component to the remaining diffuse cloud $D$ of the source environment one finds that all combinations occur in the sample: There are 5 objects with a highly concentrated inner source ($C \geq 58\%$) embedded in a massive surrounding cloud ($D \geq 67\%$). There are several objects, which have a rather flat central source distribution ($C \leq 46\%$) with a relatively weak diffuse environment ($D \leq 39\%$). Four objects are without a diffuse environment at all.

Apart from HH 7-11, which appears to be a triple source, the compact components can be approximated by Gaussians, whose deconvolved major and minor axes $a$ and $b$ have been determined with a formal accuracy between 0.4 and 1.5″. This, and a possible elevation dependent change in the beam shape of the IRAM 30 m, which, however, should be always better than $a/b$ = 1.2, leads us to introduce a safe limit of $a/b$ = 1.5 below which we consider the components to be of spherical shape. Ratios $a/b > 1.5$ indicate an elongated structure. Whether this is due to additional fainter sources or to a real flattened dust distribution can not be distinguished with the present spatial resolution. It seems plausible, however, that contours which are asymmetric with respect to the minor axes are likely to indicate multiple embedded sources whereas symmetric contours are more in favour of a non–spherical dust configuration. With these remarks we note that there are 17 spherical and 10 elongated sources; the corresponding ratios $a/b$ are contained in Table 1 (column 7).

We have compared the orientation of the dust major axes for the 10 elongated sources with that of the corresponding optical HH flow. Even allowing for large errors in the determination of the orientation of the dust major axis we find no correlation at all, i.e. the relative angles of the flattened dust configurations and the HH flows are distributed between 0 and 90 degrees. This suggests that the collimation of the flows must occur on much smaller scales than what can be achieved with an 11″ beam.

## 5. Conclusions

1. We have presented 1300 $\mu$m continuum maps of the environment of 20 HH energy sources. The dust emission arises from a compact component surrounded by a diffuse envelope. The relative contributions of both components to the total flux from the area varies from very compact to rather diffuse sources.
2. Half of the sources show a flattened shape of the dust emission contours. The orientations of these ellipsoids are not correlated to the optical jet axes of the HH flows.
3. Within the HH 114 region we have detected a new mm–continuum source (HH 114 MMS) with a rather flat ($\beta \sim 1$) SED from 350 to 2000 $\mu$m. Its ratio $L_{bol}/L_{smm} \sim 90$ qualifies this source as Class 0.
4. Within the HH 1-2 region there are four mm–sources. MMS1 corresponds to the double source VLA 1/2 driving the HH 1-2 and HH 144 flows. There is a fainter ridge 17″ to the SSW of MMS1, located in a dense lobe of the flattened $NH_3$ structure surrounding MMS1. MMS2 is associated with the VLA sources found near an $H_2O$ maser SW of HH 1. A fainter source, MMS3, is found about 20″ SSW of MMS2; both of these sources are associated with an extended $NH_3$ cloud. In the north–eastern part of the region we see the mm emission from the energy source of HH 147.
5. Close to the driving source of HH 108-109 we have detected a new mm–continuum source (HH 108 MMS) which we suggest to be a further protostellar candidate.
6. In the region of HH 7-11 we have detected three mm sources. MMS1 and MMS2 coincide with two mm sources previously detected by Grossman et al. (1987) while MMS3 is new. Comparison with the VLA observations of Rodríguez et al. (1997) suggests that their VLA 2 and our MMS3 coincide, and that their VLA 3 and our MMS1 are identical. The coincidence of a strong mm source with VLA 3 supports the suggestion of Rodríguez et al. (1997) that VLA 3, rather than SVS 13, is the driving source of the HH 7-11 outflow.

*Acknowledgements.* We want to thank our referee Dr. P. Abraham for a number of valuable suggestions which improved the manuscript in several aspects.

## References

André Ph., Ward-Thompson D., Barsony M. 1993, ApJ 406, 122
Aspin C., Sandell G., Russell A.P.G., 1994, AA Suppl. 106, 165
Bally J., Devine D., Reipurth B., 1996, ApJL 473, L49
Beichman C.A., Neugebauer G., Habing H.J., Clegg P.E., Chester T.J.(eds), 1988, 'IRAS Explanatory Supplement', NASA RP-1190, Washington
Cernicharo J., 1991, in The Physics of Star Formation and Early Stellar Evolution, Eds. C.J.Lada, N.D.Kylafis, Kluwer, p.287
Chini R., Krügel E., Haslam C.G.T., et al., 1993, A&A 272, L5
Cohen M., Schwartz R.D., 1979, ApJ 233, L77
Cohen M., Harvey P.M., Schwartz R.D., 1985, ApJ 296, 633
Davis C.J., Dent W.R.F., Burnell S.J.B., 1990, MNRAS 244, 173
Duncan W.D., Robson E.I., Ade P.A.R., Griffin M.J., Sandell G., 1990, MNRAS 234, 126
Eislöffel J., Mundt R., Böhm K.-H., 1994, AJ 108, 1042
Griffin M.J., Orton G.S. 1993, Icarus 65, 244
Grossman E.N., Masson C.R., Sargent A.I., et al., 1987, ApJ 320, 356
Haro G., 1952, ApJ 115, 572
Harvey P.M., Joy M., Lester D.F., Wilking B.A., 1986, ApJ 301, 346
Haschick A.D., Moran J.M., Rodríguez L.F., et al., 1980, ApJ 237, 26
Haschick A.D., Moran J.M., Rodríguez L.F., Ho, P.T.P., 1983, ApJ 265, 281
Herbig, G.H., 1951, ApJ 113, 697

Herbig G.H., Jones B.F., 1983, AJ 88, 1040
Koo B.-C., 1989, ApJ 337, 318
Lo K.Y., Burke B.F., Haschick A.D., 1975, ApJ 202, 81
Marcaide J.M., Torrelles J.M., Güsten R., et al., 1988, A&A 197, 235
Martin-Pintado J., Cernicharo J., 1987, A&A 176, L27
Orton G.S., Griffin M.J., Ade P.A.R., et al., 1986, Icarus 67, 289
Pravdo S.H., Rodríguez L.F., Curiel S., et al., 1985, ApJ 293, L35
Pravdo S.H., Chester T.J., 1987, ApJ 314, 308
Reipurth B., 1994, A general catalogue of Herbg–Haro objects, electronically published via anon.ftp to ftp.hq.eso.org, directory /pub/Catalogs/Herbig–Haro
Reipurth B., Eiroa C., 1992, AA 256, L1
Reipurth B., Chini R., Krügel E., Kreysa E., Sievers A., 1993a, AA 273, 221
Reipurth B., Heathcote S., Roth M., Noriega-Crespo A., Raga A.C., 1993b, ApJ 408, L49
Reipurth B., Nyman L.-Å., Chini R., 1996, A&A 314, 258
Reipurth B., Bally J., Devine D., 1997, AJ, in press
Rodríguez L.F., Cantó J., Torrelles J.M., Anglada G., Ho P.T.P., 1990a, in Formation of Stars and Planets and the Evolution of the Solar System, ESA-SP 315, p.179
Rodríguez L.F., Ho P.T.P., Torrelles J.M., Curiel S., Cantó J., 1990b, ApJ 352, 645
Rodríguez L.F., Reipurth B., 1996, Rev. Mexicana Astron.Astrofis. 32, 27
Rodríguez L.F., Anglada G., Curiel S., 1997, ApJL, in press
Roth M., Tapia M., Rubio M., Rodríguez L.F., 1989, AA 222, 211
Sandell G. 1994, MNRAS 271, 75
Sandell G., Aspin C., Duncan W.D., Robson E.I., Dent W.R.F., 1990, A&A 232, 347
Solf J., Böhm K.-H., 1987, AJ 93, 1172
Solf J., Böhm K.-H., Raga A.C., 1989, ApJ 305, 795
Stevens J. A., Robson E.I., 1994, MNRAS, 270, L75
Strom S.E., Vrba F.J., Strom K.M., 1976, AJ 81, 314
Strom S.E., Strom K.M., Grasdalen G.L., et al., 1985, AJ 90, 2281
Torrelles, J.M., Cantó, J., Rodríguez, L.F., Ho, P.T.P., Moran, J.M., 1985, ApJ 294, L117
Torrelles J.M., Gómez J.F., Ho P.T.P., et al., 1993, ApJ 417, 655
Ward-Thompson D., Robson E.I., Whittet D.C.B., et al., 1989, MNRAS, 241, 119
Ward-Thompson D., Robson E.I., 1990, MNRAS, 244, 458
Ward-Thompson D., Chini R., Krügel E., André P., Bontemps S., 1995, MNRAS, 274, 1219
Woody D.P., Scott S.L., Scoville N.Z., et al., 1989, ApJ 337, L41

This article was processed by the author using Springer-Verlag LaTeX A&A style file *L-AA* version 3.